Received 1 March 2015
Revised 7 August 2015
Accepted 29 August 2015

Analysis and determination of mechanical bearing load caused by unbalanced magnetic pull

Andreas Ruf, Michael Schröder, Aryanti Kusuma Putri, Roman Konrad, David Franck and Kay Hameyer
Institute of Electrical Machines, RWTH Aachen University, Aachen, Germany

Abstract

Purpose – The purpose of this paper is to focus on the mechanical bearing load caused by the unbalanced magnetic pull (UMP), which is studied in detail. The applied approach is based on an analysis of static and dynamic eccentricities at different positions and different amplitudes. The influence of the operating points is calculated to show the effective bearing load for machines operating at different speeds. The decreasing lifetime of the applied bearings is examined and evaluated in detail.

Design/methodology/approach – To evaluate the proposed methodology a permanent magnet synchronous machine (PMSM) with buried magnets is used. To consider effects of slotting and saturation, a finite element (FE) model is employed. The Monte Carlo method is used to determine the most likely amplitudes of the eccentricities. Calculating the UMP for all possible operating points using a control strategy for the machine and coupling this results with a drive cycle, determines the effective force acting on the bearing.

Findings – It has been shown that the position of the eccentricity has a not significant influence on the behavior of the UMP and may therefore be neglected. The amplitude of the eccentricity vector influences the amplitude of the UMP including all harmonic force components. For technical relevant eccentricities, the influence is approximately linear for the average and the dominant harmonics of the UMP. In most cases, it is sufficient to displace the rotor at an arbitrary position and amplitude. It is sufficient to simulate one type of eccentricity (static or dynamic) with an arbitrary value of displacement (rotor or stator) to evaluate all possible airgap unbalances. Using stochastic simulations of the eccentricity amplitudes enables an a priori design and lifetime estimation of bearings.

Originality/value – This paper gives a close insight on the effect of mechanical bearing load caused by rotor eccentricities. The effect of the position of the eccentricity vector, the operational range and a drive cycle are considered. A stochastic simulation and an empirical lifetime model of one bearing gives an example of using this methodological approach.

Keywords Electrical machines, Eccentricity, PMSM, Bearing load, Lifetime, Unbalanced magnetic pull

Paper type Research paper

1. Introduction

Electrical drives in industrial and automotive applications are manufactured by mass production. Hence, deviations caused by the production such as displacements of the bearing seats, uneven rotor magnetization (Novak and Kosek, 2014), or displacements of the rotational axis of the rotor are unavoidable as described in Smith and Dorrell (1996), Frauman *et al.* (2007) and Dorrell *et al.* (2013). Amongst others, these lead to a rotor eccentricity and causes an unbalanced magnetic pull (UMP), which mechanically burdens the bearings. One widely applied approach to estimate this additional stress on the bearings is an electromagnetic worst case simulation of a particular operating point.

The results presented in this paper have been developed in a research project granted by the Federal Ministry for Economic Affairs and Energy with the reference number 01MY12006A.

COMPEL: The International Journal for Computation and Mathematics in Electrical and Electronic Engineering
Vol. 35 No. 2, 2016
pp. 728-743

0332-1649
DOI 10.1108/COMPEL-03-2015-0111

Further studies investigate the influence of slot and pole number combinations (Zhu *et al.*, 2013) and excitation using analytic models (Wu *et al.*, 2010). The most sophisticated approach is to consider the operating range of the machine in addition. Therefore, in this paper a method is developed that allows to combine a finite element model to calculate the UMP for different current excitation and the specific control strategy to incorporate the operation characteristics of the machine to create a more sophisticated base for the approximation of the occurring forces. Coupling these results with a drive cycle and a lifetime model, the effective acting force on the bearings can be determined to estimate the expected lifetime.

2. Theory

The magnetic flux density in the airgap of an electrical machine:

$$B(\alpha, t) = \Theta(\alpha, t) \cdot \Lambda(\alpha, t) \tag{1}$$

is calculated from the magnetomotive force $\Theta(\alpha, t)$ and the magnetic permeance $\Lambda(\alpha, t)$, where α is an angular position in the airgap of the machine and t is a moment in time. For a uniform airgap the permeance can be described by:

$$\Lambda = \frac{\mu_0}{\delta_\mathrm{m}}, \tag{2}$$

with the vacuum permeability μ_0 and the uniform airgap length δ_m (Seinsch, 1992). Due to slotting of stator or rotor, static or dynamic eccentricities, or saturation of the magnetic materials in the electrical machine, the airgap can not be assumed as constant.

To consider these effects, the simple magnetic permeance from Equation (2) is multiplied by specific permeances λ:

$$\Lambda(\alpha, t) = \frac{\mu_0}{\delta_\mathrm{m}} \cdot \lambda_\mathrm{S} \cdot \lambda_\mathrm{R} \cdot \lambda_\mathrm{SE} \cdot \lambda_\mathrm{DE} \cdot \lambda_\mathrm{sat}\,. \tag{3}$$

Stator and rotor slotting as well as saturation are considered by the specific permeances λ_S, λ_R and λ_sat respectively and can be determined as described in Seinsch (1992) and Oberretl (2007).

Eccentricity occurs in rotating machines when the stator's center is not in the same position as the rotor's center. The effects of eccentricity are considered by λ_SE and λ_DE. Figure 1 schematically illustrates an eccentric machine with the stator center M, the stator inner radius R, the rotor center S and the rotor radius r. The displacement between M and S is the eccentricity $e = \overline{MS}$ of the machine.

Depending on the position of the rotating axis the eccentricity is dynamic or static. For the case that the rotation axis is at the position of the rotor center S, the eccentricity is called static eccentricity and the position of the smallest airgap length remains at one location around the circumference. For the other case, if the rotation axis is at the position of the stator center M, the center of the rotor rotates on the dashed circle. The eccentric motion is called dynamic eccentricity and the position of the smallest airgap revolves. In general, both types of eccentricity may occur at the same time and lead to a mixed eccentricity.

With the average airgap length $\delta_\mathrm{m} = R - r$, the relative eccentricity ε can be expressed as:

$$\epsilon = \frac{e}{R - r} = \frac{e}{\delta_\mathrm{m}}. \tag{4}$$

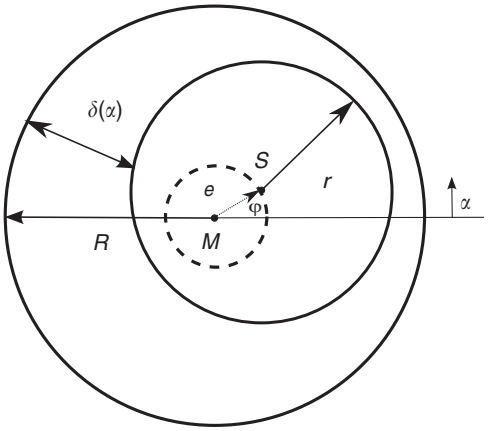

Figure 1.
Schematic model for the airgap calculation of an eccentric rotating machine

For practically relevant eccentricities $\delta_m \ll R$, the airgap length $\delta(\alpha)$ can be determined for the case of static eccentricity as:

$$\delta(\alpha) = \delta_m \cdot (1 - \epsilon \cdot \cos(\alpha - \varphi)), \tag{5}$$

where α is the angular position in the airgap and φ the angle of the eccentricity.

For the case of dynamic eccentricity, the airgap length $\delta(\alpha, t)$ becomes dependent on time:

$$\delta(\alpha, t) = \delta_m \cdot (1 - \epsilon \cdot \cos(\alpha - \omega t - \varphi)), \tag{6}$$

where ω is the angular frequency of the rotor.

Using this equations for the airgap length, static and dynamic eccentricity can be considered for the magnetic permeance as shown in Gieras *et al.* (2006) by using the following simplified specific permeances:

$$\lambda_{SE}(\alpha) \approx \frac{1}{\sqrt{1+\epsilon^2}} + 2 \cdot \frac{1-\sqrt{1-\epsilon^2}}{\epsilon \cdot \sqrt{1-\epsilon^2}} \cdot \cos(\alpha) \text{ and} \tag{7}$$

$$\lambda_{DE}(\alpha, t) \approx \frac{1}{\sqrt{1+\epsilon^2}} + 2 \cdot \frac{1-\sqrt{1-\epsilon^2}}{\epsilon \cdot \sqrt{1-\epsilon^2}} \cdot \cos(\omega t - \alpha). \tag{8}$$

The magnetic flux density in the airgap of an electrical machine from Equation (1) is a vector quantity and can be divided into its two components $B_{rad}(\alpha, t)$ and $B_{tan}(\alpha, t)$ – the radial and the tangential component. The force density at the intersection between the machine's airgap and the stator can be derived from the Lorentz force and simplified by means of the Maxwell stress tensor. This results in the well-known equations for the tangential component of the force density:

$$\sigma_{tan}(\alpha, t) = \frac{1}{\mu_0} \cdot B_{rad}(\alpha, t) \cdot B_{tan}(\alpha, t) \tag{9}$$

and the radial component (Smith and Dorrell, 1996):

$$\sigma_{\mathrm{rad}}(\alpha,t)=\frac{1}{2\mu_0}\cdot\left(B_{\mathrm{rad}}^2(\alpha,t)-B_{\mathrm{tan}}^2(\alpha,t)\right)$$

$$\approx\frac{1}{2\mu_0}\cdot B_{\mathrm{rad}}^2(\alpha,t). \tag{10}$$

The relative magnetic permeability μ_r of the ferromagnetic material in an electrical machine is much higher than that of the airgap (e.g. $\mu_{r,Fe}\approx 10{,}000\gg\mu_{r,Air}\approx 1$). With this assumption the magnetic flux lines run predominantly in radial direction through the airgap, so that the radial flux density $B_{\mathrm{rad}}(\alpha,t)$ is much higher than the tangential one $B_{\mathrm{tan}}(\alpha,t)$. This results in the simplified approximation in Equation (10) (Gieras *et al.*, 2006). The tangential force density σ_{tan} is necessary for the torque production in the electrical machine. The integral over the tangential force density along the airgap in circumferential direction yields the mechanical torque T. The major radial force density σ_{rad} acts on the stator teeth. It deforms the stator and is an essential cause of vibration and noise from electrical machines. Due to Newton's third law, the forces act also on the rotor and especially on the rotor's bearings. Integrals over the complex force density result in sum forces in x-direction:

$$F_x(t)=r\cdot l\cdot\int_0^{2\pi}\left|\underline{\sigma}(\alpha,t)\right|\cdot\cos\left(\alpha+\arg\left(\underline{\sigma}(\alpha,t)\right)\right)\mathrm{d}\alpha \tag{11}$$

and y-direction:

$$F_y(t)=r\cdot l\cdot\int_0^{2\pi}\left|\underline{\sigma}(\alpha,t)\right|\cdot\sin\left(\alpha+\arg\left(\underline{\sigma}(\alpha,t)\right)\right)\mathrm{d}\alpha \tag{12}$$

in a Cartesian coordinate system with the length l of a visualized cylinder in the machine's airgap. In a perfect symmetric electrical machine, these sum forces are zero for every time step. Sum forces unequal zero result from a difference in the air gap flux densities on opposite sides of the machine. This difference in flux density is, in general, caused by a difference in the air gap, e.g. due to rotor eccentricity. Especially crucial for the bearings are revolving sum forces, which are described by the alternating component of the sum forces – the so called unbalanced magnetic pull (UMP).

3. Calculation of the amplitude of rotor eccentricities

In order to evaluate the proposed methodology, a permanent magnet synchronous machine (PMSM) with buried magnets in the rotor is studied (Finken *et al.*, 2010). All mechanical parts in the PMSM are considered to be able to cause static or dynamic rotor eccentricities. The rotor eccentricities which lead to the UMP are determined by using the Monte Carlo method (Hartung *et al.*, 2005) and the given data in the production drawings

of the machine. Figure 2 presents the eccentricity influencing dimensional chain, which is used to calculate the distributions of the rotor eccentricities. To model each geometrical manufacturing deviation in the tolerance fields M_i, a truncated normal distribution with 10^6 elements is applied:

$$f(x,\mu,\sigma)=\frac{e^{\left(\frac{(x-\mu)^2}{-2\sigma^2}\right)}}{\int_0^\infty e^{\left(\frac{(x-\mu)^2}{-2\sigma^2}\right)}}\cdot I_{[a,b]}(x)=\begin{cases}0 & x\le 0\\ \dfrac{e^{\left(\frac{(x-\mu)^2}{-2\sigma^2}\right)}}{\int_0^\infty e^{\left(\frac{(x-\mu)^2}{-2\sigma^2}\right)}} & x>0.\end{cases} \tag{13}$$

In the industrial area the processes are controlled by defining control limits. Nowadays the standard interval width between the process control limits is 8σ. Thereby, in this paper the tolerance limits correspond to an interval width of 8σ and μ is centered in the interval. For the discussed PMSM the stochastic parameters for all deviations are $\mu = 25\,\mu m$ and $\sigma = 6.25\,\mu m$. After superposing all deviations, the statistically most likely rotor eccentricity is determined. In Figure 3 kernel smoothed functions are presented which were derived from the histograms which contain 10^6 cases of eccentricity.

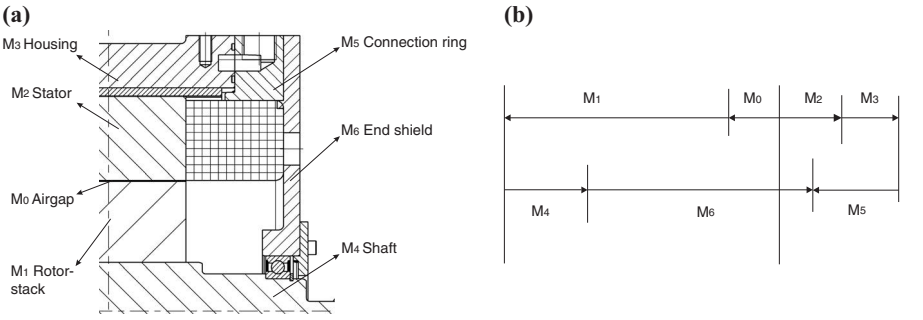

Figure 2. Eccentricity influencing dimensional chain

Notes: (a) Machine drawing; (b) dimensional chain

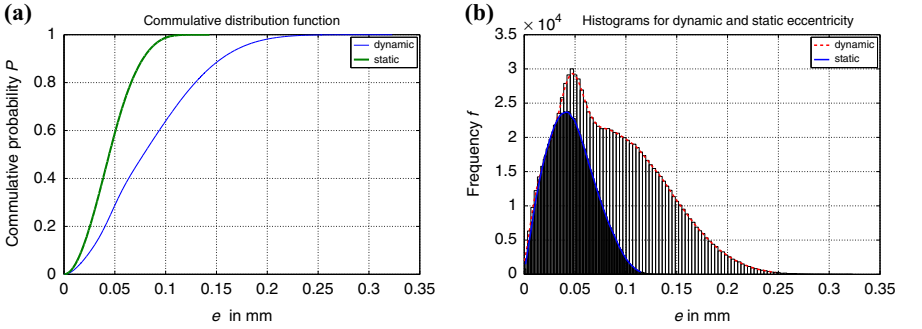

Figure 3. Distribution of the static and dynamic rotor eccentricities for 10^6 simulated deviations

Notes: (a) Commulative probability; (b) probability distribution

4. Calculation of operating points

The following section introduces a methodology to incorporate the operation characteristics in the simulation of electrical machines.

The electrical machine is modeled in a rotor-flux-fixed dq-reference frame including cross coupling magnetization and saturation (Herold *et al.*, 2011):

$$\begin{bmatrix} \hat{\Psi}_\mathrm{d} \\ \hat{\Psi}_\mathrm{q} \end{bmatrix} = \begin{bmatrix} L_\mathrm{dd} & L_\mathrm{dq} \\ L_\mathrm{qd} & L_\mathrm{qq} \end{bmatrix} \begin{bmatrix} \hat{i}_\mathrm{d} \\ \hat{i}_\mathrm{q} \end{bmatrix} + \begin{bmatrix} \hat{\Psi}_\mathrm{f,d} \\ \hat{\Psi}_\mathrm{f,q} \end{bmatrix}. \tag{14}$$

The quadrature current i_q and direct current i_d are varied during the simulation to extract the average torque determined by the eggshell method (Henrotte *et al.*, 2004) for different excitation. The flux-linkage vector is calculated with the geometrical summation:

$$\hat{\Psi} = \sqrt{\hat{\Psi}_\mathrm{d}^2 + \hat{\Psi}_\mathrm{q}^2}. \tag{15}$$

In order to calculate the operating points for the whole operating range, a combined control strategy is used. The optimization problem is defined by:

$$\begin{aligned} \underset{\hat{i}_{\mathrm{d},i,j}, \hat{i}_{\mathrm{q},i,j} \in \mathbb{R}}{\text{minimize}} \quad & \mathrm{J}(\hat{i}_{\mathrm{d},i,j}, \hat{i}_{\mathrm{q},i,j}) = \sqrt{\hat{i}_{\mathrm{d},i,j}^2 + \hat{i}_{\mathrm{q},i,j}^2} \\ \text{subject to} \quad & T_i = \tfrac{3}{2} p \left(\hat{\Psi}_{\mathrm{d},i} \hat{i}_{\mathrm{q},i} - \hat{\Psi}_{\mathrm{q},i} \hat{i}_{\mathrm{d},i} \right), \quad \forall\ i = 1, \ldots, m \\ & \hat{u}_j = \omega_j \hat{\Psi}_i \le \hat{u}_\mathrm{max}, \qquad \forall\ j = 1, \ldots, n \end{aligned}$$

with the torque vector $T_1, T_2, \ldots, T_m$ subject to $m \in \mathbb{N}$ and the speed vector $n_1, n_2, \ldots, n_n$ with $n \in \mathbb{N}$. This optimization problem combines the maximum torque per ampere (MTPA) control for the base speed range and the maximum torque per voltage (MTPV) control for the field weakening range (De Doncker *et al.*, 2010).

Figure 4 shows the trajectories of the average electromagnetic torque calculated with different current excitations. Further an overlaid mesh of calculated operating points ($f_\mathrm{el} = [0\ \mathrm{Hz}, 400\ \mathrm{Hz}], T_\mathrm{el} = [0\ \mathrm{Nm}, 220\ \mathrm{Nm}]$), using the combined control strategy,

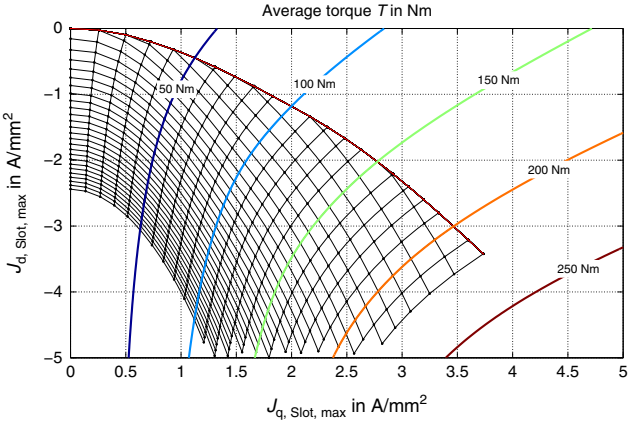

Figure 4. Simulated map of the average torque with overlaid mesh of operating points

is mapped. The rotor-flux-oriented current vectors are defined by the operating points, which are calculated for the given optimization problem. The basic speed range is represented by the trajectory that extends along the rising torques (MTPA-line), whereas the field weakening area is represented by the mesh below this trajectory. Figure 5 illustrates the direct and quadrature current component speed-torque map for the entire operating range for a maximum amplitude of the induced voltage of $\hat{u}$= 360 V. These defined dq-current combinations are used to calculate the UMP for each operating point in the entire operating range of the PMSM.

5. Calculation of the unbalanced magnetic pull

In order to evaluate the influence of dynamic and static eccentricity on the behavior of the UMP, different positions of the smallest airgap of the eccentricity vector are modeled. In Figure 6 different directions of the eccentricity vector are shown for dynamic (a) and static (b) eccentricity. These directions are used to evaluate the influence of the radial position of eccentricity on the UMP. For dynamic eccentricity three positions and for static eccentricity two positions are compared.

To consider effects of slotting and saturation, a finite element (FE) model is employed. To determine the forces caused by eccentricity on the machine's behavior the Eggshell method (Henrotte *et al.*, 2004) is employed. Figure 7(a) illustrates the computation result of the electromagnetic forces on the circumference of the rotor.

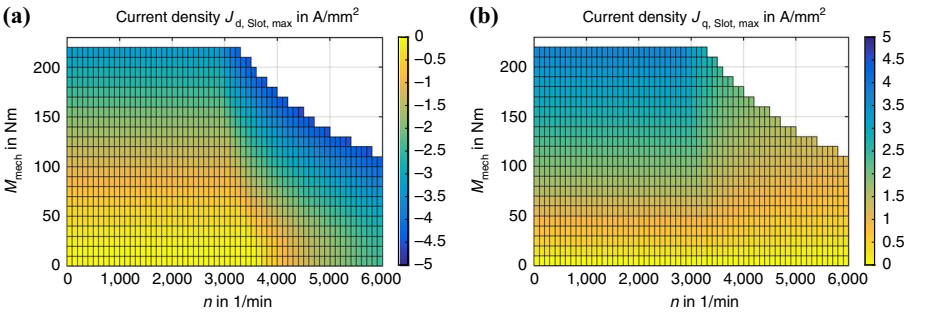

Figure 5.
Current density in dq-reference frame for different operating points

Notes: (a) Direct current densitiy per slot; (b) quadrature current density per slot

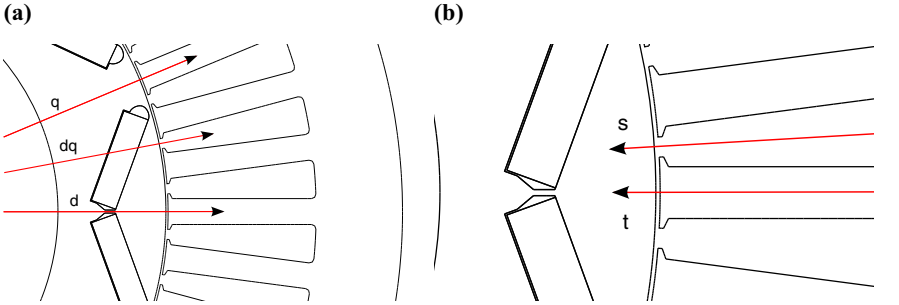

Figure 6.
Simulated positions of rotor eccentricity in dq-reference frame

Notes: (a) Dynamic rotor eccentricity; (b) static rotor eccentricity

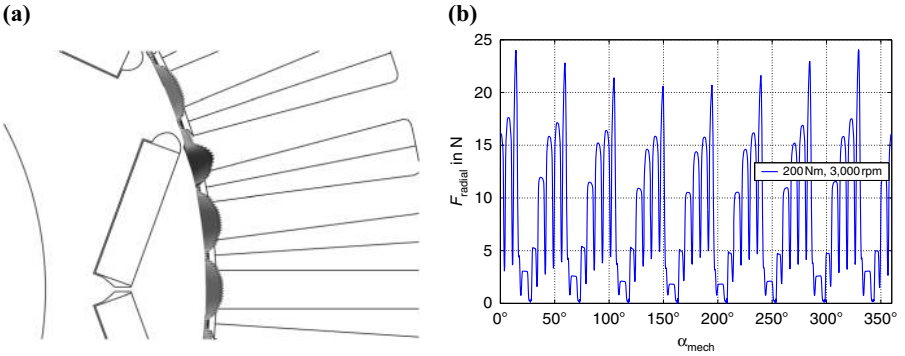

Notes: (a) Force vectors on the circumference; (b) radial component of the force vectors

Figure 7. Electromagnetic forces on the circumference of the rotor ($\epsilon = 2/7$)

These forces are decomposed into a tangential and a radial component. The radial component of these electromagnetic forces is presented in Figure 7(b). The radial force consists of the slot harmonics with $N = 48$, the order of the poles $2p = 8$ and the harmonic order caused by the varying permeance through the eccentricity $N_{ex} = 1$. The radial forces are integrated along the circumference of the rotor in order to calculate the unbalanced magnetic pull. This is done for each position of the rotor at rotor-fixed-coordinate frame for dynamic eccentricity and stator-fixed-coordinate frame for static eccentricity. The rotation-angle-dependent behavior of the UMP will be evaluated afterwards. The presented operating points in Section 3 are used to calculate the UMP for different current excitation in the entire operational range of the used PMSM. To study the influence of the eccentricity angle of the rotor, the positions of the eccentricity are varied according to Figure 6.

6. Results

6.1 Dynamic eccentricity

The influence of the direction of the eccentricity vector is presented in Figure 8. From that figure can be concluded that the position of the eccentricity has insignificant

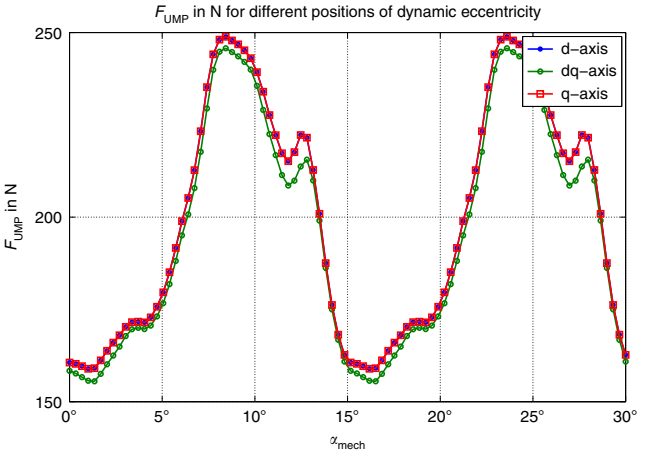

Figure 8. UMP vs the mechanical angle for different positions of the eccentricity vector

influence on the UMP. The UMPs caused by the displacements in d- and q-axis are identical. The UMP between the axes is only slightly lower than the first. The amplitude and the harmonics are effected by the specific permeance of the rotor λ_R. In case of a PMSM with buried permanent magnets, the rotor has no slots and the specific permeance is only influenced by the geometry of the stator. As illustrated in Figure 8, the specific permeance of the rotor has a minor effect when compared to the slot harmonics of the stator.

In Figure 9 the effects of rising amplitude of the eccentricity vector on the amplitude of the UMP are illustrated. The increase in the eccentricity effects a nearly linear increase of the average and all harmonics of the UMP in the range of practically occurring eccentricity amplitudes (Figure 10).

A tolerance analysis of the electrical machine used in the simulation has revealed that the most likely eccentricity is in the range of $e = 50$ µm i.e. $\epsilon = 1/14$ ($\delta_m = 700$ µm). For this reason, the following results are presented for this amplitude of the eccentricity vector in order to make the results more comprehensible.

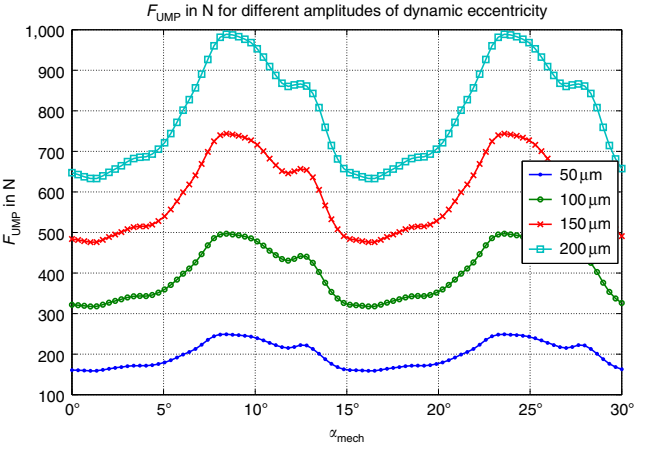

Figure 9.
UMP as a function of the mechanical angle for different amplitudes of the eccentricity vector ($\delta_m = 700$ µm)

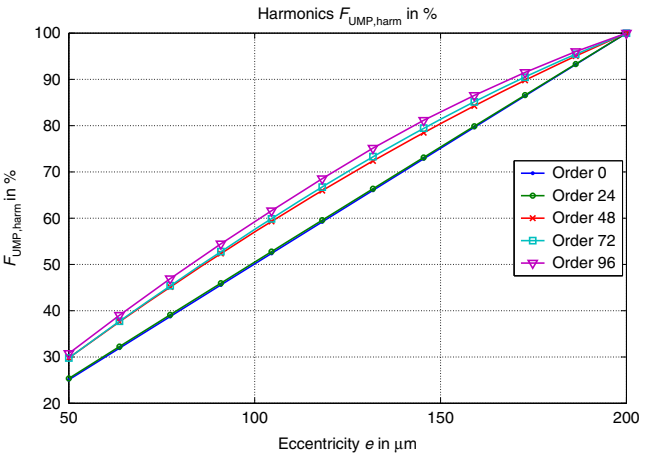

Figure 10.
Harmonics of the UMP as a function of the amplitude of the eccentricity vector ($\delta_m = 700$ µm)

Figure 11(a) shows the calculated average UMP and the operating points for different current excitations. It is apparent that the UMP depends on the position of the flux linkage, relative to the position of the eccentricity vector. Starting from the no-load point, the average of the UMP increases with the increase of the quadrature current and the negative direct current. Depending on the quadrature current the average UMP reaches its maximum, while depending on the direct current the UMP increases continuously.

Figure 11(b) illustrates the average UMP in the speed-torque map. The maximum of the average UMP depending on the quadrature current can also been seen in base speed range of the machine at 55 Nm. In the field weakening range, the quadrature current decreases for a given torque and the direct current increases. This effects an increase of the UMP up to the maximum for the whole speed-torque map. The results for the harmonic component of the UMP are presented in Figure 12(a) and (b).

The harmonic component is a distinctive proportion of the UMP and increases in direction of increasing quadrature current and direct current. However, the increase depending on the direct current dominates also for the harmonic component. In the speed-torque map, the harmonic component (Figure 12(b)) has also its maximum at high frequency and high torques. In the base speed range the harmonic component increases with increasing torque almost continuously. In the area of low torque the harmonic component is modest.

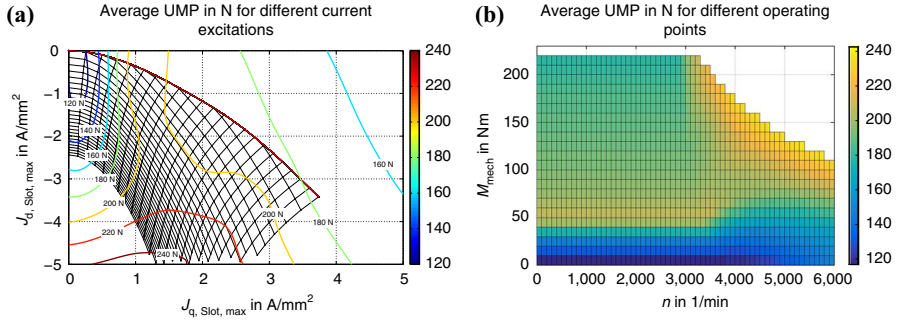

Figure 11.
Average UMP

Notes: (a) Operating points; (b) speed-torque map

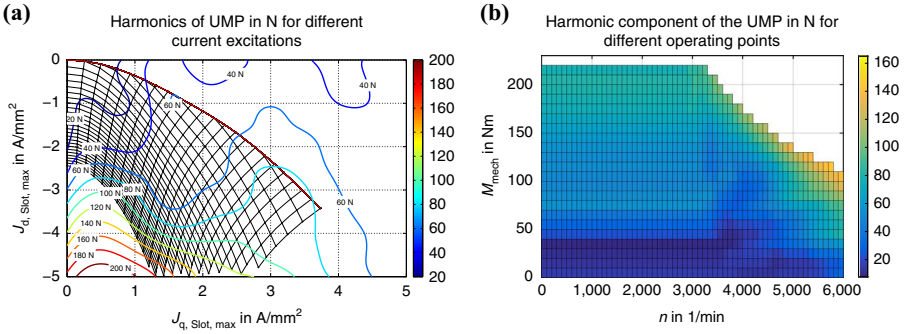

Figure 12.
Harmonic component of the UMP

Notes: (a) Operating points; (b) speed-torque map

Figure 13(a) presents the behavior of the UMP as a function of the rotation angle of the rotor for two chosen operating points: at nominal point ($n = 3{,}000$ rpm, $T = 200$ Nm) and at maximum flux weakening point ($n = 6{,}000$ rpm, $T = 100$ Nm).

The UMP at 6,000 rpm has a higher harmonic and average component than the UMP at 3,000 rpm. The harmonic components of both operating points are shown in Figure 13(b). The UMP harmonics for the operating point at maximum flux weakening are generally higher than the nominal operating point. This is caused by the higher proportion of direct current, which leads to a higher UMP, as shown in Figures 11 and 12. The orders 24 and 48 are the dominant harmonics for both operating points. The order 48 is caused by the stator slotting and the harmonic component 24 by saturation.

The dependencies of these harmonic components are shown in Figure 14. Both components are increasing with the increase of the direct current. The order 24 is also dependent on the quadrature current, while the order 48 caused by stator slots is almost independent of the quadrature current.

6.2 Static eccentricity

The calculation of the static eccentricity is analogous to the method described for the dynamic eccentricity. The UMP is calculated by integration of the radial force density on the circumference of the rotor. Figure 15 presents the UMP caused by static eccentricity in rotor-fixed frame, calculated for the nominal point ($n = 3{,}000$ rpm, $T = 200$ Nm).

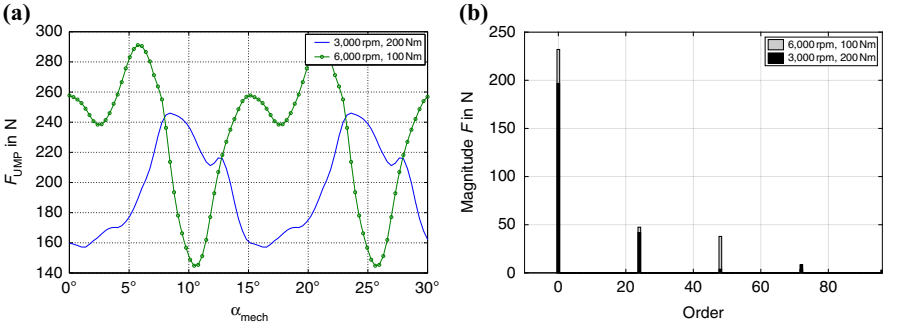

Figure 13. UMP for two different operating points

Notes: (a) UMP vs the mechanical angle; (b) orders of the force magnitude

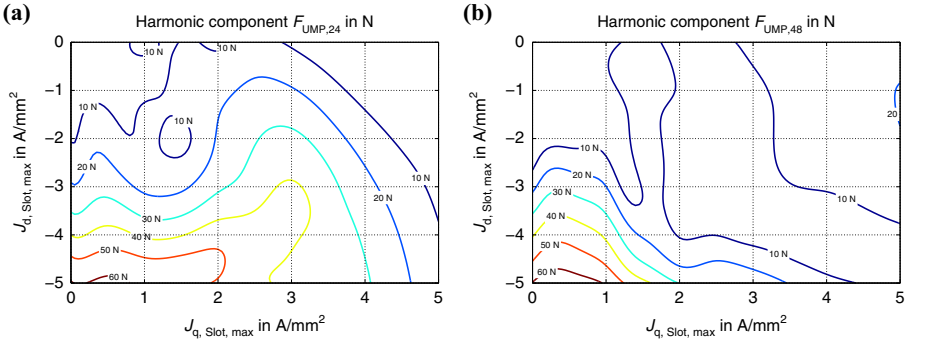

Figure 14. Simulated maps of harmonic components

Notes: (a) Harmonic component 24; (b) harmonic component 48

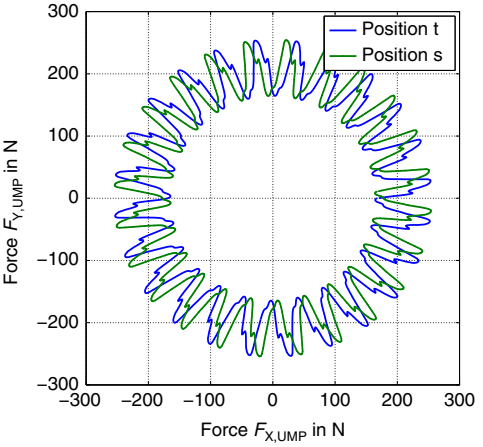

Figure 15.
UMP caused by static eccentricity in rotor fixed reference frame for position t and s (e = 50 µm)

The UMP acts in the direction of the smallest air gap. This position of the air gap rotates from the perspective of the rotor, and therefore the UMP is also rotating. The difference in the position of the static eccentricity only influences the angular position of the UMP. For both cases the orders 24 and 48 are dominant, caused as described by stator slotting and saturation. In order to describe the behavior in time domain, the UMP is transformed to the point of smallest airgap in the stator-fixed frame.

Comparing the results presented in Figures 11 and 12 for the dynamic eccentricity, the stator currents are varied for the same eccentricity amplitude $e = 50$ µm e.g. $\epsilon = 1/14$ and decomposed into an average and harmonic component. The results are illustrated in Figure 16.

It can be seen that the results differ in a negligible extent. An examination of the harmonics distribution gives the same result as shown in Figure 14.

6.3 Bearing lifetime estimation

The additional loads for the bearings due to the UMP have a significant impact on the bearing lifetime. In the ideal case, no axial loads are applied to the bearings. Therefore, axial forces are not taken into account. To consider the effect of machine usage, the

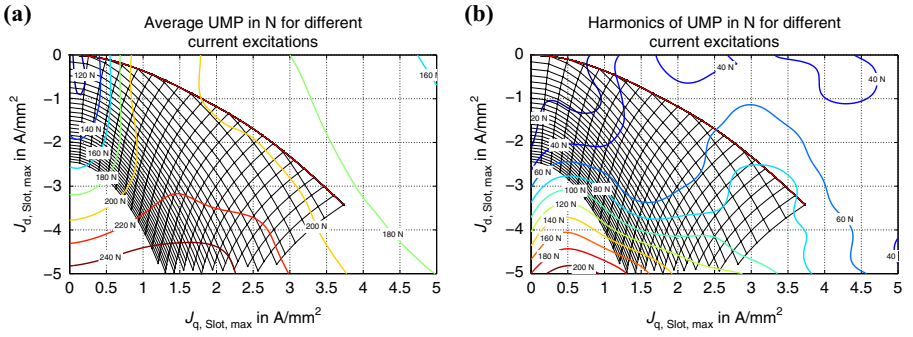

Figure 16.
Simulated maps of the UMP with overlaid mesh of operating points (static eccentricity)

Notes: (a) Average UMP; (b) harmonic component of the UMP

drive cycle WLTC Class 3 in Figure 17(a) is applied to the machine to evaluate the effective bearing load. The average UMP is calculated for 3,600 s in Figure 17(b). The equivalent dynamic bearing load P_m is determined by integration of the dynamic loads P_i for the duration t_i:

$$P_\mathrm{m} = \sqrt[3]{\frac{\sum_{i=1}^{n} P_i^3 \cdot t_i}{t}} \tag{16}$$

$$L_{10\mathrm{h}} = \frac{10^6}{60\frac{\mathrm{min}}{\mathrm{h}} \cdot n_\mathrm{m}} \cdot \left(\frac{C}{P_\mathrm{m}}\right)^3 \tag{17}$$

The nonlinear influence of high loads is considered with the exponent to the third power. n_m is the average speed and C the dynamic load rating given by the manufacturer of the bearings. Figure 18 displays the nominal bearing lifetime $L_{10\mathrm{h}}$ as a function of the equivalent dynamic load P_m (Vaculik, 2008) for two different bearings. The nominal bearing lifetime $L_{10\mathrm{h}}$ represents the duration of time in h which 90 percent

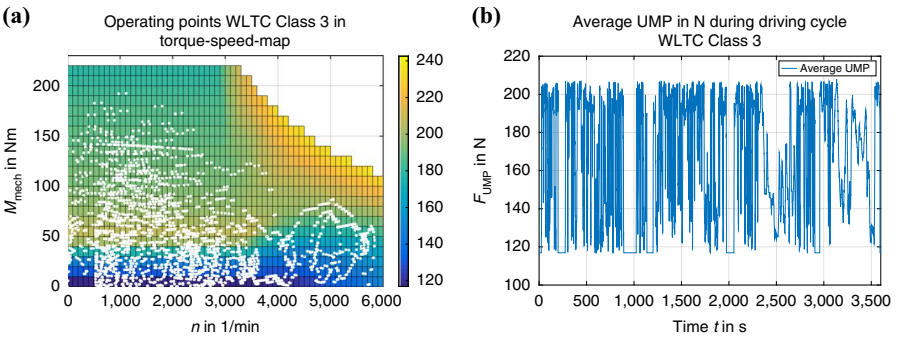

Figure 17.
UMP during drive cycle WLTC Class 3

Notes: Operating points; (b) timeseries of the average UMP for one bearing

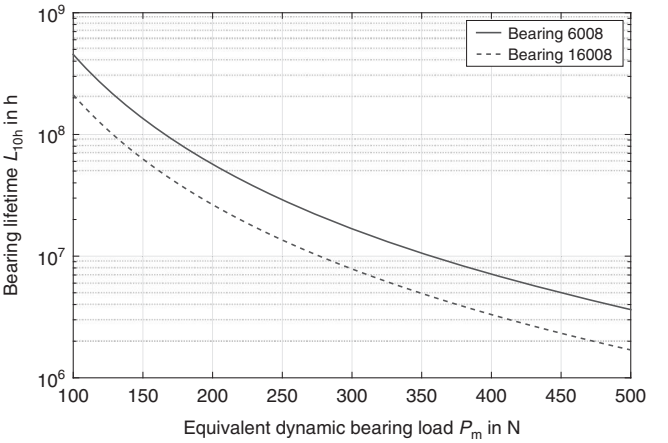

Figure 18.
Bearing lifetime $L_{10\mathrm{h}}$ as a function of the equivalent dynamic bearing load P_m

of the bearings survive. The rotor weight results in a static load of 162 N. Considering the UMP in the calculation of the equivalent dynamic bearing load of $P_{UMP} = 169.6$ N decreases the lifetime of the bearing remarkably.

For the studied prototype the originally used bearings (6008) are oversized. Depending on the drive train, additional axial loads are possible and must be considered. However, it is shown that the UMP has a large influence on the expected lifetime of the bearings.

7. Conclusion

In this paper a methodology to study the influence of the position and the amplitude of the eccentricity for the whole operating range of a PMSM is discussed. It has been shown that the position of the eccentricity has insignificant influence on the behavior of the UMP and can be therefore neglected. The amplitude of the eccentricity vector influences the amplitude of the UMP including all harmonic force components. For technical relevant eccentricities, the influence is approximately linear for the average and the dominant harmonics of the UMP. In most cases, it is sufficient to displace the rotor at an arbitrary position and amplitude. Local force distribution due to static and dynamic eccentricity reveals the same circumference but differ in their frequency components. When applying the stator fixed reference frame in case of a static eccentricity and a rotor fixed reference frame in case of a dynamic eccentricity, both types of eccentricity show the same characteristics. Therefore a transformation from static to dynamic eccentricity in the simulations and vice versa is valid. In conclusion, it is sufficient to simulate one type of eccentricity (static or dynamic) with an arbitrary value of displacement (rotor or stator) to evaluate all possible airgap unbalances. Through varying the current excitation, the UMP for all possible operating points and all possible eccentricities can be calculated with a reduced computational effort when compared to classical computation methods. This allows the application of the proposed model in stochastic simulations and enables an a priori design and lifetime estimation of bearings.

References

De Doncker, R., Pulle, D. and Veltman, A. (2010), *Advanced Electrical Drives: Analysis, Modeling, Control*, Springer, Berlin.

Dorrell, D., Hermann, A. and Jensen, B. (2013), "Analysis of unbalanced magnetic pull in wound rotor induction machines using finite element analysis – transient, motoring and generating modes, industrial electronics society", *IECON 2013-39th Annual Conference of the IEEE*, pp. 7307-7312.

Finken, T., Hombitzer, M. and Hameyer, K. (2010), "Study and comparison of several permanent-magnet excited rotor types regarding their applicability in electric vehicles", *Emobility – Electrical Power Train*, Vol. 2010, pp. 1-7.

Frauman, P., Burakov, A. and Arkkio, A. (2007), "Effects of the slot harmonics on the unbalanced magnetic pull in an induction motor with an eccentric rotor", *IEEE Transactions on Magnetics*, Vol. 43 No. 8, pp. 3441-3444.

Gieras, J.F., Wang, C. and Cho Lai, J. (2006), *Noise of Polyphase Electric Motors*, CRC Press (Taylor & Francis Group).

Hartung, J., Elpelt, B. and Klösener, K. (2005), *Statistik: Lehr- und Handbuch der angewandten Statistik; mit zahlreichen, vollständig durchgerechneten Beispielen*, Oldenbourg.

Henrotte, F., Deliége, G. and Hameyer, K. (2004), "The eggshell approach for the computation of electromagnetic forces in 2d and 3d", *COMPEL*, Vol. 23 No. 4, pp. 996-1005.

Herold, T., Franck, D., Lange, E. and Hameyer, K. (2011), "Extension of a D-Q Model of a permanent magnet excited synchronous machine by including saturation, cross-coupling and slotting effects", *International Electric Machines and Drives Conference, IEMDC 2011, Professor M.A. Rahman, Ontario, May*.

Novak, M. and Kosek, M. (2014), "Unbalanced magnetic pull induced by the uneven rotor magnetization of permanent magnet synchronous motor", *ELEKTRO*, Vol. 2014, pp. 347-351.

Oberretl, K. (2007), "Losses, torques and magnetic noise in induction motors with static converter supply, taking multiple armature reaction and slot openings into account", *Electric Power Applications, IET*, Vol. 1 No. 4, pp. 517-531.

Seinsch, H.O. (1992), *Oberfelderscheinungen in Drehfeldmaschinen – Grundlagen zur analytischen und numerischen Berechnung*, Teubner, Stuttgart.

Smith, A. and Dorrell, D. (1996), "Calculation and measurement of unbalanced magnetic pull in cage induction motors with eccentric rotors. i. Analytical model", *Electric Power Applications, IEE Proceedings*, Vol. 143 No. 3, pp. 193-201.

Vaculik, S. (2008), *A Framework for Electromechanical Actuator Design*, University of Texas at Austin, May.

Wu, L., Zhu, Z., Chen, J. and Xia, Z. (2010), "An analytical model of unbalanced magnetic force in fractional-slot surface-mounted permanent magnet machines", *IEEE Transactions on Magnetics*, Vol. 46 No. 7, pp. 2686-2700.

Zhu, Z., Mohd Jamil, M. and Wu, L. (2013), "Influence of slot and pole number combinations on unbalanced magnetic force in pm machines with diametrically asymmetric windings", *IEEE Transactions on Industry Applications*, Vol. 49 No. 1, pp. 19-30.

About the authors

Andreas Ruf received the MSc Degree in Electrical Engineering from the Ruhr University Bochum (RUB), Germany, in August 2012. He has been working as a Research Associate at the Institute of Electrical Machines since January 2013. His research interests include iron loss computations, thermal behaviour, overload capability, lifetime models, the design and control of electrical machines. Andreas Ruf is the corresponding author and can be contacted at: Andreas.Ruf@iem.rwth-aachen.de

Michael Schröder received the Diploma Degree in Electrical Engineering from the RWTH Aachen University, Germany, in May 2012. He has been working as a Research Associate at the Institute of Electrical Machines since June 2012. He is currently working towards his Doctoral Degree in the area of noise and vibration of electrical machines.

Aryanti Kusuma Putri received the MSc Degree in Electrical Engineering from the RWTH Aachen University, Aachen, Germany, in April 2013. She has been working as a Research Associate at the Institute of Electrical Machines since June 2013. Her research interests include contactless power transmission, new arts of electrical machines, simulation and acoustical design of the electrical machines.

Roman Konrad received the Diploma Degree in Mechanical Engineering from the RWTH Aachen University, Germany, in April 2013. He has been working as a Research Associate at the Institute of Electrical Machines since July 2013. His research interests include manufacturing processes for electrical machines, analysis and modelling of manufacturing deviations and mathematical methods.

David Franck received the Diploma Degree in Electrical Engineering from the RWTH Aachen University, Aachen, Germany, in 2008. After that he became staff (Research Associate) at the Institute of Electrical Machines. Since 2011 he has been working as a Chief Engineer of the Institute of Electrical Machines. His main field of research is the acoustic behaviour of electrical machines.

Dr Kay Hameyer received his Diploma Degree in Electrical Engineering from the University of Hannover and his PhD Degree from the Berlin University of Technology, Germany. After his university studies he worked with the Robert Bosch GmbH in Stuttgart, Germany, as a Design Engineer for permanent magnet servo motors and vehicle board net components. Until 2004 Dr Hameyer was a full Professor for Numerical Field Computations and Electrical Machines with the KU Leuven in Belgium. Since 2004, he is a Full Professor and the Director of the Institute of Electrical Machines (IEM) at the RWTH Aachen University in Germany. In 2006 he was vice dean of the faculty and from 2007 to 2009 he was the dean of the faculty of Electrical Engineering and Information Technology of RWTH Aachen University. His research interests are numerical field computation and optimisation, the design and controls of electrical machines, in particular permanent magnet excited machines, induction machines and the design employing the methodology of virtual reality. Since several years Dr Hameyer's work is concerned with the magnetic levitation for drive systems, magnetically excited audible noise in electrical machines and the characterisation of ferro-magnetic materials. Dr Hameyer is author of more than 250 journal publications, more than 500 international conference publications and author of four books. Dr Hameyer is a member of VDE, IEEE senior member, fellow of the IET.